ROYAL SOCIETY
OF CHEMISTRY

Check for updates

A versatile core–shell hetero-nanostructure catalysed chemo-selective synthesis of β-enamino carbonyl compounds†

Sriparna Dutta,[ab] Prashant Kumar,[c] Shivani Sharma,[ad] Sneha Yadav,[a] Priyanka,[a] Ranjana Dixit,[ad] Anju Srivastava[ab] and Rakesh Kumar Sharma [ID] *[a]

A core–shell hetero-nanostructure comprising a new *in situ* generated naphthoquinone cobalt complex covalently immobilized on a silica coated magnetite nanosupport has been described for catalyzing the enamination of β-carbonyl compounds. The newly developed catalyst works as a nanoreactor for boosting this reaction and provides unprecedented chemoselective access to the targeted β-enaminoesters as well as β-enaminones. The synergistic covalent incorporation of an organic entity (a flexible spacer) onto an inorganic solid (surface modified support material) imparts a considerable structural rigidity to the catalyst thereby preventing leaching of the active catalytic species as well evidenced by the hot filtration experiment. Elemental survey and core level XPS spectra confirm the presence of the +II oxidation state of cobalt which is the active catalytic species. This work throws light on how catalytic activity can be tuned and "activity, selectivity and recyclability" the three desired features of a green catalyst can be accomplished on a single platform through careful manipulation of interaction between the support material and active metal complex.

Sustainability spotlight

In 2015, the entire world came to a common consensus when seventeen sustainable development goals were outlined by the various member countries of the UN that carried a vision of rendering the planet safer for all. With a very few years left to accomplish these goals, tremendous efforts will be required to transform the commitments into action. Catalysis the key principle of green chemistry provides one of the most promising and logistic routes for achieving most of the SDGs such as zero hunger, good health & well being, clean water & sanitation, affordable & clean energy, industries, innovation & infrastructure, responsible consumption & production and climate action. The present work discloses the design of a novel core–shell hetero nanostructure based catalyst comprising a new *in situ* generated naphthoquinone cobalt complex covalently immobilized on a silica coated magnetite nanosupport that has unveiled promising outcomes in catalyzing the enamination of β-carbonyl compounds (that synergistically integrate the nucleophilicity of the enamine and electrophilicity of the enone functionalities, thereby serving as valuable synthons for the construction of essential pharmaceutical drugs). Although literature reports document the development of several synthetic approaches involving homogeneous metal complexes that provide access to these compounds, yet appealing generality and the scope of industrial utility of these catalytic protocols are vitiated by the fact that most of them rely on homogeneous metal salts as catalysts that are not only difficult to recover from the reaction mixture but also major contributors to metal contamination. The present work is a sustainable attempt to overcome the serious limitations of previous protocols *via* the establishment of a catalyst that offers "activity, selectivity and recyclability" the three desired features of a green catalyst in a single platform through careful manipulation of interaction between the support material and active metal complex.

Introduction

The drive towards cleaner and sustainable chemical manufacturing has led to a reassessment of many of the existing catalytic technologies. Today, there is a renewed focus on the development of green catalytic systems that exhibit higher activity as well as enhanced reusability as they provide a potent solution to meet the current challenges of energy and sustainability. In fact, with the booming of nanotechnology, it has been possible to design such efficient catalysts as they allow the precise engineering of finer structural details of catalysts such as size, shape and surface properties.[1–5] Although efforts in this direction have enabled the successful generation of interesting nanomaterials suited for various applications, magnetically responsive nanomaterials have, in particular, shown great promise in the field of catalysis owing to their riveting physico-chemical properties.[6–12] Magnetic nanoparticles work as excellent solid support materials for the design of superior and well-

[a]Green Chemistry Network Centre, Department of Chemistry, University of Delhi, Delhi-110007, India. E-mail: rksharamgreenchem@hotmail.com

[b]Department of Chemistry, Hindu College, University of Delhi, Delhi-110007, India

[c]Department of Chemistry, SRM University Delhi-NCR, Sonepat, Haryana-131029, India

[d]Department of Chemistry, Ramjas College, University of Delhi, Delhi-110007, India

tuned heterogeneous nanocatalysts that exhibit high activity and selectivity similar to their homogeneous counterparts.[13,14] Nanosized particles dramatically increase the net exposed surface area of the active component of the catalyst, eventually resulting in improved product yield. Besides, most importantly, these catalysts show a rapid response towards an external magnetic field that ensures their ready separation from the reaction mixture using an external magnetic device. Magnetic field assisted separation is green, economical and undoubtedly an attractive alternative to tedious, time-consuming filtration techniques. Thus, researchers have devoted an enormous amount of attention towards the synthesis of these magnetically recyclable nanocatalysts. However, an obvious deterioration in their activity as a consequence of strong agglomeration tendency of the magnetic nanoparticles has raised serious concerns.[15,16] In order to address this issue, core–shell magnetic silica based nanomaterials comprising nanoparticles suitably encapsulated within a layer of silica have been developed as they uniquely combine the characteristic features of the magnetic core as well as the silica shell that screens the dipolar attraction between the individual particles, thereby preventing their aggregation.[17–20] In addition, the silanaceous coat also allows free access to various chemical species from outside, rendering them suitable for catalytic applications. The efficacy of silica encapsulated magnetic nanoparticle supported catalytic systems has prompted us to come up with a new core–shell structured magnetic silica supported cobalt nanocatalyst for the synthesis of unsaturated β-carbonyl moieties such as β-enaminones and β-enaminoesters.

β-Enaminones and β-enaminoesters represent well documented scaffolds that have fuelled the research interest of several organic chemists worldwide as they synergistically integrate the nucleophilicity of the enamine and electrophilicity of the enone functionalities, thereby serving as valuable synthons for the construction of essential pharmaceutical drugs.[21–24] Besides, they constitute prevalent structural motifs of biologically significant natural products that are endowed with a broad spectrum of interesting pharmacological properties such as antibacterial, anticonvulsant, anti-inflammatory, antitumour *etc.*[25–31] Thus, over the past few decades a number of captivating strategies have been reported for obtaining these heterocyclic moieties which include reactions of β-enaminoesters with organolithium reagents,[32] addition of amide enolates or metallic esters to imidoyl halides,[33–36] nitriles,[37–39] and tosylimines[40,41] and addition of enamines or ketamines to activated carboxylic acid derivatives.[42–44] However, despite the existence/prevalence of a large number of intriguing protocols in the literature, the classical approach involving the direct condensation of amines with 1,3-dicarbonyls still continues to be one of the most widely pursued pathways for the synthesis of β-enamino ketones and esters because of its operational simplicity and higher atom economy.[45] Consequently, a wide array of catalysts such as Sc(OTf)$_3$,[46] Zn(OAc)$_2$·6H$_2$O,[47] ZrOCl$_2$·8H$_2$O,[48] Ca(CF$_3$COO)$_2$,[49] CoCl$_2$,[50] InBr$_3$,[51] I$_2$,[52] silica gel,[53] CeCl$_3$·7H$_2$O[54] and NaAuCl$_4$[55] have been employed proficiently to afford this transformation. Unfortunately, the appealing generality and the scope of industrial utility of these catalytic protocols are vitiated by the fact that most of them rely on homogeneous metal salts as catalysts that are not only difficult to recover from the reaction mixture but also major contributors to metal contamination. Thus, in consideration of growing economic and industrial concerns, it is extremely imperative to develop other alternative environmentally benign, heterogeneous recyclable catalytic systems that can efficiently conquer the challenges of β-enaminone and β-enaminoester synthesis.

In a quest to design a supreme catalytic route for obtaining these industrially and biologically significant β-enamine based moieties and engaged in the development of organic–inorganic hybrid catalysts for various organic transformations, we herein report the fabrication, characterization and application of a promising core–shell magnetic silica based cobalt nanocatalyst (Co-NQ@Am-SiO$_2$@Fe$_3$O$_4$). The newly developed catalytic system enables the generation of a diverse range of β-enaminones and β-enaminoesters with excellent turnover numbers and high product selectivity under neat reaction conditions at room temperature. Apart from this, the ease of catalytic retrievability *via* magnetic attraction and outstanding recycling efficiency (observable up to eight consecutive runs) render the present protocol a practical alternative to all previously established methodologies for the synthesis of β-enamine ketones and esters. To the best of our knowledge, this is the first report wherein a magnetically retrievable nanocatalyst has been designed and subsequently utilized for the enamination of β-ketoesters and β-ketones.

Experimental

Materials and reagents

1,2-Naphthoquinone (1,2-NQ) (97%), tetra-ethyl orthosilicate (TEOS) (99.9%) and 3-aminopropyltriethoxysilane (APTES) (98%) were purchased from Alfa Aesar, Sigma Aldrich and Fluka, respectively. Ferrous sulphate, ferric sulphate and cobalt chloride hexahydrate salts were commercially acquired from Sisco Research Laboratory (SRL). The rest of the synthetic reagents were procured from Spectrochem Pvt Ltd and were used as received without further purification.

Characterization techniques

The crystallographic structure and phase of the synthesized nanomaterials were analyzed well with the help of the powder X-ray diffraction (PXRD) technique which was performed using a Bruker, D8 Advance (Karlsruhe, Bundesland, Germany) diffractometer with Cu/Kα radiation at a scanning rate of 4° min^{-1} in the 2θ range of 5–80° (λ = 0.15405 nm, 40 kV, 40 mA). Electron microscopic techniques such as transmission electron microscopy (TEM) and field emission scanning electron microscopy (FE-SEM) were carried out in order to determine the size, shape and purity of the nanocomposites. TEM was conducted using a JEOL 2100F, and FE-SEM images were obtained with the aid of a Tescan Mira 3 FE-SEM instrument. The energy-dispersive X-ray spectroscopic technique (equipped with the SEM instrument) was utilized for the detailed compositional analysis of the nanocomposites. Coloured elemental

mapping images were also obtained using the same instrument. The XPS survey spectrum of the catalyst and the core-level spectra of Fe 2p and Co 2p were procured with the help of a K-Alpha™+ X-ray photoelectron spectrometer system. The fitting of the core level spectra was performed by adjusting the baseline relative to the signal background. The chemically distinct species were resolved using a Gaussian distribution fitting procedure with peak positions, and areas were determined. The stepwise modifications of the magnetite nanoparticles were identified by Fourier transform infrared (FT-IR) spectroscopy. The FT-IR spectra of the various stages of the nanocatalyst were acquired through a PerkinElmer Spectrum 2000 FT-IR spectrometer that utilized the KBr pellet method and was operative in the range of $4000–400$ cm^{-1} under atmospheric conditions with a resolution of 1 cm^{-1}. In order to extract information about the magnetic properties of the nanocomposites, a vibrating sample magnetometer (EV-9, Microsense, ADE) was used. The presence of cobalt in the final nanocatalyst was affirmed through energy dispersive X-ray fluorescence (ED-XRF) spectroscopy using a Fischerscope X-ray XAN-FAD BC. Thereafter, the amount of cobalt loaded onto surface modified magnetite nanoparticles was estimated *via* flame atomic absorption spectroscopy (FAAS) on a Labindia AA 7000 atomic absorption spectrometer. Prior to AAS analysis, the microwave assisted digestion of the catalyst was performed in an Anton Paar Multiwave 3000 microwave reaction system equipped with a temperature and pressure sensor. A sonicator (Tekmar Sonic Disruptor model TM300) was utilized for dispersing the nanoparticle aggregates in ethanol. The GC-MS analysis of the synthesized products was carried out on an Agilent gas chromatograph (6850 GC) with an HP-5MS 5% phenyl methyl siloxane capillary column (30.0 m $\times$ 250 μm $\times$ 0.25 μm) and a quadrupole mass filter equipped 5975 mass selective detector (MSD) using helium as carrier gas (rate 0.9 mL min^{-1}).

Catalyst preparation

Synthesis of amine functionalized silica encapsulated magnetite nanoparticles. At first, the synthesis of magnetite (Fe_3O_4) nanoparticles was carried out in accordance with the literature reported co-precipitation method.[56] Typically, 6.0 g of ferric sulphate and 4.2 g of ferrous sulphate salts were dissolved in 250 mL double distilled water and stirred at 60 °C until a yellowish orange coloured solution was obtained. Subsequently, 25% NH_4OH was added to it dropwise so as to alter the pH of the solution to 10 and the stirring was continued for almost an hour. The crystalline black precipitate of Fe_3O_4 nanoparticles was isolated magnetically, washed well with deionized water and ethanol and dried under vacuum. Once the bare Fe_3O_4 nanoparticles were synthesized, a modified sol–gel strategy was adopted for the silica encapsulation of the magnetically responsive core material.[57] This step involved the ultrasonic dispersion of the magnetite nanoparticles (1.0 g) for approximately 30 minutes, followed by the addition of ammonia (6.0 mL) and TEOS (2.0 mL), respectively. The resultant reaction mixture was stirred at room temperature continuously for 24 h which resulted in the formation of a brownish black precipitate of the silica coated magnetite nanoparticles ($SiO_2@Fe_3O_4$). These $SiO_2@Fe_3O_4$ nanoparticles were segregated *via* magnetic attraction, washed thoroughly with ethanol several times and dried under vacuum. Thereafter, the surface functionalization of the modified nanoparticles was carried out by adding APTES (5.0 mL) to ultrasonically dispersed $SiO_2@Fe_3O_4$ nanoparticles (1.0 g) in ethanol (200 mL). The obtained amine functionalized silica encapsulated magnetite nanoparticles ($Am-SiO_2@Fe_3O_4$) were separated again using an

Magnetic silica based organic-inorganic hybrid cobalt nanocatalyst
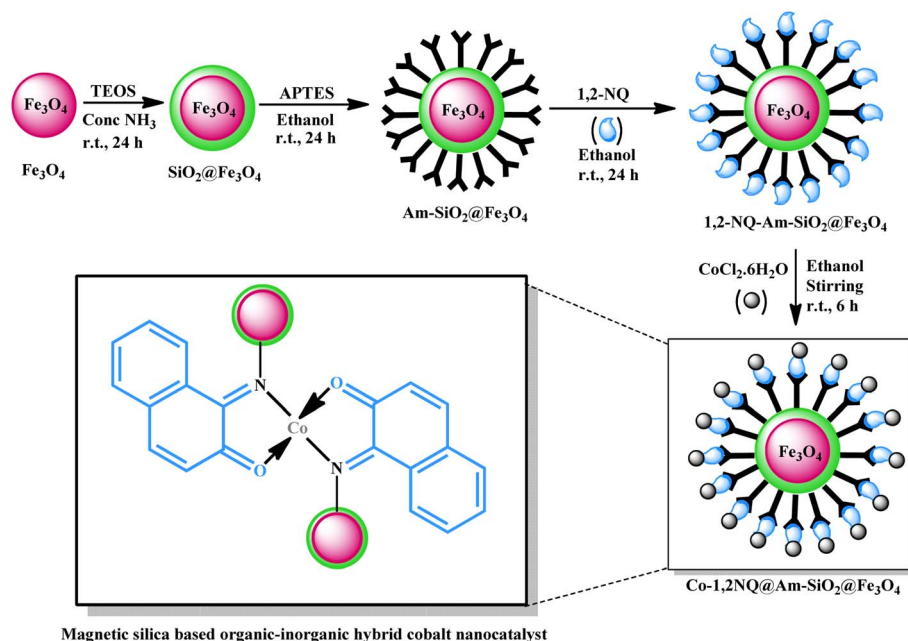
Scheme 1 Schematic illustration of the synthesis of Co-NQ@Am-SiO₂@Fe₃O₄ nanocatalyst.

external magnet, washed repeatedly with ethanol to eliminate any unreacted silylating agent and then dried under vacuum.

Synthesis of the Co-NQ@Am-SiO$_2$@Fe$_3$O$_4$ nanocatalyst. The synthesis of the final nanocatalyst was achieved in two steps. First, the ligand was immobilized onto the amine functionalized silica encapsulated magnetite nanosupport. For obtaining ligand grafted surface modified magnetite nanoparticles (NQ@Am-SiO$_2$@Fe$_3$O$_4$), a mixture of Am-SiO$_2$@Fe$_3$O$_4$ (1.0 g) and 1,2-naphthoquinone (2 mmol) was stirred in 250 mL ethanol solution at room temperature for 24 hours.[58] Next, the NQ@Am-SiO$_2$@Fe$_3$O$_4$ nanoparticles were metallated using cobalt chloride hexahydrate. In this step, NQ@Am-SiO$_2$@Fe$_3$O$_4$ (1.0 g) was stirred with a solution containing 2 mmol of cobalt chloride hexahydrate dissolved in ethanol for 6 h. The synthesized nanocomposites were carefully isolated with the help of an external magnet, washed well with ethanol and finally dried under vacuum (Scheme 1).

General procedure for the Co-NQ@Am-SiO$_2$@Fe$_3$O$_4$ catalyzed synthesis of β-enaminones and β-enaminoesters. To a solution containing amine (1 mmol) and a β-dicarbonyl compound (1 mmol), the Co-NQ@Am-SiO$_2$@Fe$_3$O$_4$ nanocatalyst (20 mg) was added and the resultant reaction mixture was subjected to stirring at room temperature (25 °C) under solvent free conditions for an appropriate period of time. Upon completion of the reaction as indicated by thin layer chromatography (TLC), the catalyst was retrieved using a bar magnet. Thereafter, the reaction contents were extracted several times with ethyl acetate (3 × 10 mL) and dried over Na$_2$SO$_4$. Finally, the synthesized heterocyclic products were confirmed and analyzed by GC-MS.

Results and discussion

Catalyst characterization

Morphological attributes of the bare and surface modified magnetite nanoparticles were investigated with the help of electron microscopic tools such as Transmission Electron Microscopy (TEM) and Scanning Electron Microscopy (SEM). The representative TEM and SEM images of the synthesized nanocomposites are depicted in Fig. 1. It is quite evident from the TEM micrograph of the core material (Fe$_3$O$_4$) that it consists of tiny particles of nearly spherical morphology with an average diameter lying between 8 and 12 nm. The selected area electron diffraction (SAED) pattern of Fe$_3$O$_4$ reveals the high crystallinity of these nanoparticles by showing the presence of a well pronounced array of diffraction rings arising from the planes of magnetite. For their detailed structural analysis, high resolution transmission electron microscopy (HR-TEM) was also conducted. The HR-TEM image of the pristine Fe$_3$O$_4$ nanoparticles clearly illustrates the 2D lattice fringes that correspond to the (220) plane of the inverse spinel structured magnetite with an interplanar separation value of 0.28 nm. Besides providing a significant amount of knowledge about the size, shape and crystallinity of the Fe$_3$O$_4$ nanoparticles, TEM and SEM also work as powerful tools for identifying the differences between the bare and modified magnetite nanoparticles. As shown in Fig. S1†, these nanoparticles acquire core–shell
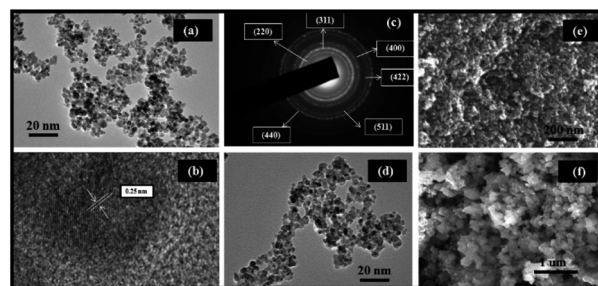

Fig. 1 (a) TEM image of nano-Fe$_3$O$_4$; (b) HR-TEM image of nano-Fe$_3$O$_4$; (c) SAED pattern of nano Fe$_3$O$_4$; (d) TEM image of the Co-NQ@Am-SiO$_2$@Fe$_3$O$_4$ nanocatalyst; (e) FE-SEM image of Fe$_3$O$_4$ and (f) FE-SEM image of the Co-NQ@Am-SiO$_2$@Fe$_3$O$_4$ nanocatalyst.

morphology after being suitably coated with amorphous silica. A closer examination of this image reveals that the core material is embedded deep within the silane shell, which makes it a good core–shell nanomaterial. Furthermore, the deposition of various surface modifying species on these SiO$_2$@Fe$_3$O$_4$ nanoparticles is verified from the obtained TEM micrograph of the final nanocatalyst. The FE-SEM images of the various nanocomposites procured at high magnification divulge a change in the surface topography of the magnetic nanocore. On being subjected to several synthetic modifications, the smooth surface of the naked Fe$_3$O$_4$ nanoparticles apparently gets transformed into a rough one which may be attributed to the deposition of silica in the core–shell structured nanomaterials. However, the possibility of precipitation of primary silica nanoparticles is certainly excluded as no separate colloidal aggregates of silica can be found in the Fe-SEM images of SiO$_2$@Fe$_3$O$_4$ and Co-NQ@Am-SiO$_2$@Fe$_3$O$_4$. Finally, in order to elucidate that the catalyst maintains its efficiency even after being recycled for seven consecutive runs, the FE-SEM image of the recovered nanocatalyst has also been provided (Fig. S2†).

In order to gain an insight into the crystallinity and phase composition of the synthesized nanomaterials, wide angle powder X-ray diffraction (PXRD) measurements were performed and the typical XRD profiles of Fe$_3$O$_4$ and SiO$_2$@Fe$_3$O$_4$ are presented in Fig. 2. Interestingly, both these diffractograms
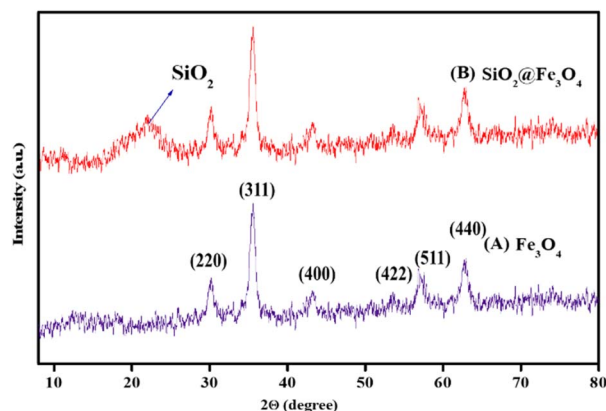

Fig. 2 XRD patterns of (a) Fe$_3$O$_4$ and (b) SiO$_2$@Fe$_3$O$_4$.

display six distinguishable Bragg's peaks at $2\theta = 30.1°$, $35.4°$, $43.1°$, $53.4°$, $57°$ and $62.6°$ that may be correctly assigned to the (220), (311), (400), (422), (511) and (440) crystallographic faces of the cubic inverse spinel structured magnetite. The peak positions as well as the relative intensities are in good agreement with the standard Fe_3O_4 XRD data as evidenced by the Joint Committee on Powder Diffraction Standards (JCPDS card: 19-629). However, the XRD pattern of silica encapsulated magnetite nanoparticles differs slightly from that of the native magnetite nanoparticles. Besides, exhibiting these well resolved diffraction peaks, the XRD spectrum of $SiO_2@Fe_3O_4$ shows the appearance of a broad diffused hump centered at around $2\theta = 23°$ which is attributed to the presence of amorphous SiO_2.[57] One aspect that needs to be highlighted here is that although the silica coating strategy efficiently leads to the generation of a protective layer of silica around the magnetic core, it does not affect the phase and purity of these crystalline nanoparticles, as evident from the diffractogram which clearly shows the retention of the six characteristic Bragg's peaks in this core–shelled nanomaterial. Furthermore, the mean crystallite size of the Fe_3O_4 nanoparticles has been evaluated using the Debye Scherrer relationship ($D_{hkl} = k\lambda l/\beta \cos\theta$) where k is a constant with a typical value of 0.89 for spherical particles, D is the average diameter in A°, β is the broadening of the diffraction line measured at half of its maximum intensity in radians, λ is the wavelength of the X-rays and θ is the Bragg diffraction angle. Choosing (311) as the reference peak, this value has been estimated to be 11.9 nm which matches well with the TEM results. Furthermore, the XRD spectra of the catalyst and the recovered catalyst, exhibiting consistency with the native ferrite peaks have been provided (Fig. S3†).

The elemental and compositional analyses of the bare and modified nanoparticles were performed using energy-dispersive X-ray spectroscopy (EDX), energy dispersive X-ray fluorescence spectroscopy (ED-XRF) and atomic absorption spectroscopy (AAS). Fig. S4† provides the EDX mapping images of the isolated particles of Fe_3O_4 and $SiO_2@Fe_3O_4$. The well resolved peaks of iron (Fe) and oxygen (O) atoms in the EDX spectrum of Fe_3O_4 affirm the presence of an iron oxide core. Besides the elemental distribution of Fe and O, the occurrence of Si in the EDX spectrum of $SiO_2@Fe_3O_4$ authenticates the successful encapsulation of the core material by silica.
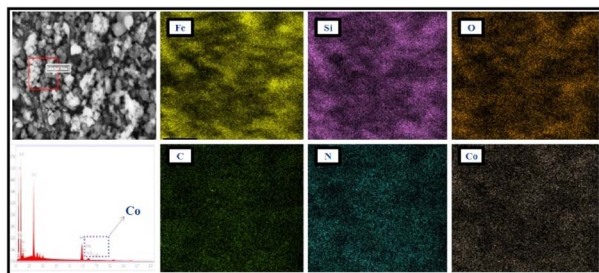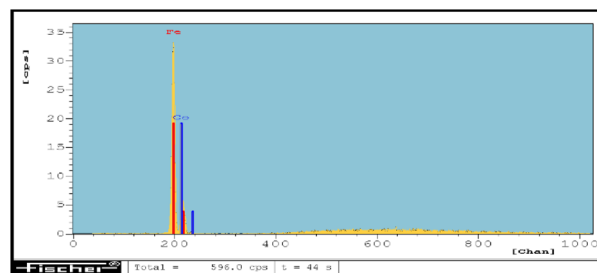

Fig. 4 ED-XRF spectrum of the Co-NQ@Am-SiO$_2$@Fe$_3$O$_4$ nanocatalyst.

Apart from this, the SEM elemental coloured mapping image of the Co-NQ@Am-SiO$_2$@Fe$_3$O$_4$ nanocatalyst (Fig. 3) has been provided which shows the presence of distinct elements – "Fe, Si, O, C, N, and Co," thus confirming the successful functionalization, ligand grafting and metallation of the silica coated magnetite nanoparticles. In addition to the elemental mapping, the ED-XRF spectrum of Co-NQ@Am-SiO$_2$@Fe$_3$O$_4$ also provides a concrete proof for the existence of the metal in the catalyst by markedly showing the presence of a sharp and distinct peak of cobalt (Fig. 4). Next, the quantitative estimation of cobalt in the prepared catalyst was performed by digesting Co-NQ@Am-SiO$_2$@Fe$_3$O$_4$ in a microwave oven at 400 W for 15 minutes with aqua regia and then subjecting the sample to AAS analysis. The corresponding metal content was evaluated to be 0.14 mmol g^{-1}.

With the aim of clearly identifying the chemical composition and acquiring information about the oxidation state of cobalt, the surface structure of the final nanocatalyst was further characterized by X-ray photoelectron spectroscopy (XPS). Fig. 5 presents the XPS elemental survey scans and core level spectra of Fe 2p and Co 2p of the magnetic silica based organic–inorganic hybrid cobalt catalyst. The presence of elements C, O, Si, N, Fe and Co is confirmed from the survey spectrum of Co-

Fig. 3 SEM elemental mapping images of the Co-NQ@Am-SiO$_2$@-Fe$_3$O$_4$ nanocatalyst showing the presence of Fe, Si, O, C, N, and Co elements.
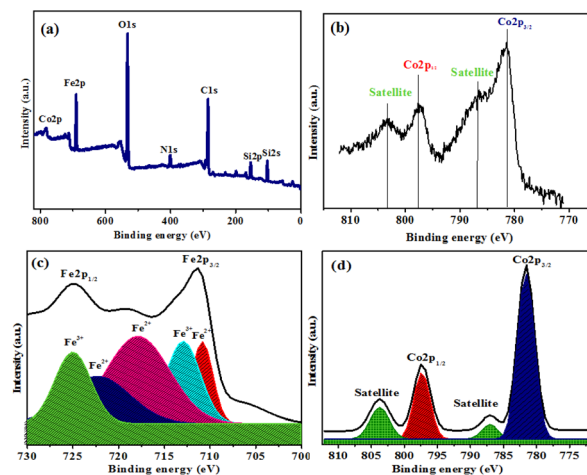

Fig. 5 (a) Survey X-ray photoelectron spectrum (XPS) of Co-NQ@Am-SiO$_2$@Fe$_3$O$_4$, (b) XPS spectra (Co 2p region) of Co in the catalyst, (c) core level XPS of Fe 2p of the sample and (d) core level XPS of Co 2p of the sample.

NQ@Am-SiO$_2$@Fe$_3$O$_4$. Next, the core level spectrum of Fe 2p was analyzed and it was found that two distinct bands appeared at around 710 and 725 eV along with a satellite peak at 717.8 eV (Fig. S5†). As these bands were broad, deconvolution of the same was attempted and successfully achieved. In the deconvoluted spectrum of Fe 2p, first the presence of combined peaks at binding energy values of 710.8 eV (Fe 2p$_{3/2}$) and 725 eV (Fe 2p$_{1/2}$) provided strong evidence of the presence of iron in the +II oxidation state in the catalyst. Furthermore, the occurrence of a satellite peak could be routinely ascribed to iron in the +II oxidation state. Apart from this, the prominent peaks appearing at binding energy values of 712 eV (Fe 2p$_{3/2}$) and 725 eV (Fe 2p$_{1/2}$) characterized the simultaneous existence of iron in the +III oxidation state in our sample. But since we are primarily interested in evaluating the oxidation state of cobalt which is the active catalytic species in our final catalyst, the XPS spectrum of Co 2p was plotted and investigated thoroughly. The deconvoluted spectrum revealed the existence of cobalt in the +II oxidation state. In this case, the binding energies for the two possible spin states 781.2 eV and 797.5 eV are responsible for 2p$_{3/2}$ and 2p$_{1/2}$ transitions, respectively and in addition, two satellite peaks were observed which primarily arose from each of the 2p transition.

For the structural confirmation of the various nanocomposites through functional group detection, Fourier transform infrared (FT-IR) spectroscopic analysis was carried out at room temperature. Fig. 6 depicts the FT-IR spectra of Fe$_3$O$_4$, SiO$_2$@Fe$_3$O$_4$, Am-SiO$_2$@Fe$_3$O$_4$, NQ@Am-SiO$_2$@Fe$_3$O$_4$ and Co-NQ@Am-SiO$_2$@Fe$_3$O$_4$.

The FT-IR spectrum of Fe$_3$O$_4$ exhibits a sharp and intense absorption band at 595 cm^{-1} indicative of typical Fe–O stretching vibrations and a relatively less intense broad band centered at 3149 cm^{-1} corresponding to the vibrations of OH groups present on the surface of the magnetite nanoparticles.[59] These characteristic absorption bands collectively provide strong evidence for the formation of the Fe$_3$O$_4$ nanocore. Next, the existence of the silane shell around this core is affirmed from the spectrum of SiO$_2$@Fe$_3$O$_4$ which distinctly shows the

presence of Si–O–Si symmetric, Si–O–Si asymmetric and Si–O symmetric stretching modes appearing at 806, 954 and 1102 cm^{-1} respectively.[60] Furthermore, the proof for the successful integration of the functionalizing agent "APTES" into the coated nanoparticles is provided by the appearance of two new bands at 2930 cm^{-1} and 1625 cm^{-1} that can be assigned to the CH$_2$ and NH$_2$ groups of the aminopropyl moiety. On moving towards NQ@Am-SiO$_2$@Fe$_3$O$_4$, a distinctive band of C=N stretch is observed at 1646 cm^{-1} besides the expected absorption bands which suggests that the ligand has been successfully immobilized over the surface of the amine functionalized silica coated ferrite nanoparticles. Astonishingly, as a result of complexation between the nitrogen atom and the metal, the value of the C=N stretch is shifted to a lower wavenumber (1630 cm^{-1} from 1646 cm^{-1}) in the case of the final nanocatalyst.

In order to examine the magnetic properties of the synthesized nanocomposites, a vibrating sample magnetometer (VSM) was employed and the resultant magnetization curves of Fe$_3$O$_4$, SiO$_2$@Fe$_3$O$_4$ and Co-NQ@Am-SiO$_2$@Fe$_3$O$_4$ recorded within the field range of $-20\,000$ to 20 000 Oe at 300 K are displayed in Fig. 7. The hysteresis loops of these powdered nanomaterials reveal the absence of any remanence or co-ercivity phenomena which confirms their superparamagnetic properties at room temperature. Besides, the inset also supports this observation as the obtained plots clearly show that both the magnetization and demagnetization curves pass through the origin. Furthermore, the value of saturation magnetization (Ms) of the prepared Fe$_3$O$_4$ nanoparticles as estimated from the graph has been found to be 60 emu g^{-1} which is much lower than that of the bulk Fe$_3$O$_4$ nanoparticles. The significant reduction in the Ms value can be predominantly attributed to the presence of disordered spins on the surface of the nanoparticles that prevent the core spins from aligning along the field direction, thereby causing a net decrease in the saturation magnetization of the small sized nanoparticles. Additionally, the VSM plots show a gradual decrement in the Ms values on moving from the bare Fe$_3$O$_4$ to the surface modified Fe$_3$O$_4$ (*i.e.* Fe$_3$O$_4$ >
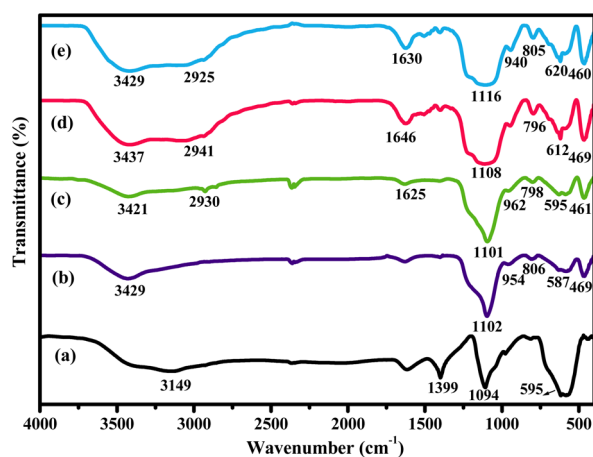
Fig. 6 FTIR spectra of (a) Fe$_3$O$_4$; (b) SiO$_2$@Fe$_3$O$_4$; (c) Am-SiO$_2$@Fe$_3$O$_4$; (d) NQ@Am-SiO$_2$@Fe$_3$O$_4$ and (e) Co-NQ@Am-SiO$_2$@Fe$_3$O$_4$.
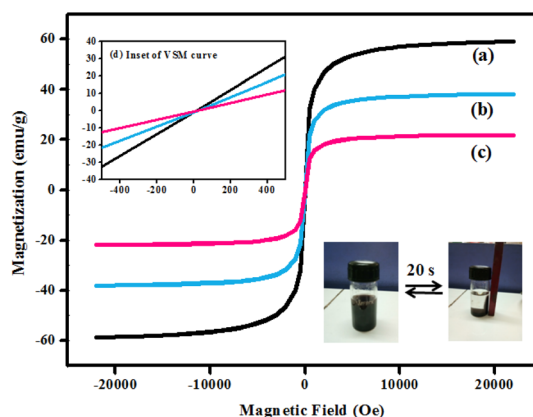
Fig. 7 Magnetization curves obtained by VSM at room temperature for (a) Fe$_3$O$_4$, (b) SiO$_2$@Fe$_3$O$_4$, and (c) Co-NQ@Am-SiO$_2$@Fe$_3$O$_4$ and (d) inset: an enlarged image near the coercive field.

SiO$_2$@Fe$_3$O$_4$ > Co-NQ@Am-SiO$_2$@Fe$_3$O$_4$) which may be ascribed to the existence of non-magnetic materials on the surface of the core–shelled nanoparticles.[61] However, it is worth mentioning here that regardless of the lowering of the saturation magnetizations, the redispersibility and magnetic properties of the final nanocatalyst remain unaffected and the Co-NQ@Am-SiO$_2$@Fe$_3$O$_4$ nanoparticles are easily retrieved from the reaction mixture with the help of a bar magnet within a very short span of time.

Investigation of catalytic activity of Co-NQ@Am-SiO$_2$@Fe$_3$O$_4$ in the synthesis of β-enaminones and β-enaminoesters
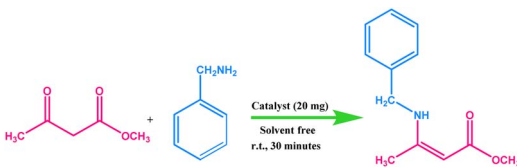
The efficacy of the newly prepared magnetic silica-based cobalt nanocatalyst was evaluated in the synthesis of industrially significant β-enaminone and β-enaminoester moieties. For achieving the best catalytic results, the effects of some of the crucial thermodynamic and kinetic reaction parameters such as catalyst concentration, time, temperature, solvents and molar substrate ratio were investigated in detail. We commenced our study by choosing methyl acetoacetate and benzylamine as the model substrates.

The quest for establishing optimal reaction conditions began by performing the catalytic screening test. However, at the outset, to truly assess the significance of a catalyst in the enamination reaction, a control experiment was conducted with the test substrates in the absence of a catalyst. A careful evaluation of the outcome divulged that only traces of the expected product could be detected under such experimental conditions (Table 1, entry 1). Next, a wide range of cobalt based catalysts were screened sequentially for the generation of the desired β-enaminoester scaffold with a high conversion percentage. Gratifyingly, as shown in Table 1, amongst all the tested cobalt

sources, the developed Co-NQ@Am-SiO$_2$@Fe$_3$O$_4$ and Co-based catalysts formed by the coordination of CoCl$_2$ with 1,2-naphthoquinone (Co-NQ complex) prove to be the most proficient ones, exhibiting the best catalytic activity by causing a 100% conversion of the employed reactants. In comparison to the precursor CoCl$_2$ salt utilized for the reaction which gave 95% conversion and the other salts such as CoSO$_4$ and CoBr$_2$ that showed very low activity (42% and 45%, respectively) the Co-NQ complex gave a higher conversion that could be ascribed to the coordinating effect of 1,2-naphthoquinone with CoCl$_2$, leading to a robust and active complex. Furthermore, although Co-NQ and Co-NQ@Am-SiO$_2$@Fe$_3$O$_4$ showed similar conversions, yet the fabricated catalyst "Co-NQ@Am-SiO$_2$@Fe$_3$O$_4$" emerged as the material of choice owing to the exceptional magnetism conferred by the material which enhanced the catalytic recoverability and reusability properties. Subsequently, in order to analyse the effect of catalyst concentration, the reactions were performed by varying the amount of catalyst from 5 to 20 mg and the results have been demonstrated in Table 1. It was found that an increase in the catalyst loading caused a substantial improvement in the conversion percentage of the product from 39% to 100% which could be attributed to the simultaneous increase in the active catalytic sites. Thus, for the rest of the studies, the amount of the catalyst was fixed at 20 mg.

After optimization of the amount of catalyst, our next investigation was focussed on addressing the influence of the substrate molar ratio on the reaction conversions. For an accurate assessment, three different sets of reactions were performed with 1 : 0.5, 1 : 0.75 and 1 : 1 molar ratios of methylacetoacetate and benzylamine, respectively in the presence of the Co-NQ@Am-SiO$_2$@Fe$_3$O$_4$ nanocatalyst (Fig. S6†). Apparently, the results indicated that the enamination reaction utilizing a reagent molar ratio of 1 : 0.5 could afford

Table 1 Catalyst screening test for the Co-NQ@Am-SiO$_2$@Fe$_3$O$_4$ catalyzed enamination reaction[a]

Entry	Catalyst	Yield[b] (%)	Conversion[c] (%)	TON[d]	TOF[e]
1	No catalyst	—	Traces	—	—
2	SiO$_2$@Fe$_3$O$_4$	—	Traces	—	—
3	CoSO$_4$	35	42	150	300
4	Co(OAc)$_2$	37	48	171	342
5	CoBr$_2$	40	45	161	322
6	CoCl$_2$	82	95	339	678
7	Co-NQ complex	94	100	357	714
8	Co-NQ@Am-SiO$_2$@Fe$_3$O$_4$ (5 mg)	30	39	139	278
9	Co-NQ@Am-SiO$_2$@Fe$_3$O$_4$ (10 mg)	55	68	243	486
10	Co-NQ@Am-SiO$_2$@Fe$_3$O$_4$ (15 mg)	88	95	339	678
11	Co-NQ@Am-SiO$_2$@Fe$_3$O$_4$ (20 mg)	95	100	357	714

[a] Reaction conditions: benzylamine (1 mmol), methylacetoacetate (1 mmol), catalyst (20 mg unless specified), stirring at r.t. (25 °C), no solvent. [b] Isolated Yield. [c] Conversion (%) determined by GC-MS. [d] TON is the number of moles of product per mole of catalyst. [e] TOF = TON/time (in hours).

a conversion of only 70% even after a prolonged stirring (up to 6 h) period. However, with a further increase in the molar ratio of the substrates to 1 : 1, a complete 100% conversion of the subjected reactants could be accomplished within a shorter time (30 minutes) interval. Hence, a 1 : 1 substrate molar ratio was the optimum requirement for the efficient synthesis of β-enaminones and β-enaminoesters with a good conversion percentage.

The selection of an appropriate solvent is a matter of increasing importance in the field of catalytic science and research as solvents play a key role in either facilitating or hindering a reaction through their interaction with the catalyst and the solute molecules. Thus, a scrupulous examination of the solvent effect on the enamination reaction was carried out by stirring the model reactants in the presence of solvents of variable polarities. Additionally, in consideration of the current emphasis on green, waste free synthesis, solvent free conditions were also tested, while keeping the rest of the parameters fixed. Fig. S7† illustrates the influence of solvents on the conversion percentages of the reactants. In comparison to all the non-polar solvents employed, polar solvents such as ethanol, isopropanol, acetonitrile and dimethylformamide (DMF) led to a superior reaction conversion owing to the higher solubility of the substrates in them. Notably, the best results were obtained under solvent less conditions as complete (100%) conversion of the subjected reactants was achieved in this case.

Considering the significance of temperature in altering the outcome of a reaction, we decided to investigate its effect on the one pot synthesis of β-enaminones and β-enaminoesters. As a step towards accomplishing this task, at first, the enamination reaction was performed at 25 °C using 20 mg of the synthesized Co-NQ@Am-SiO$_2$@Fe$_3$O$_4$ nanocatalyst. Thereafter, the temperature of the reaction was increased progressively at intervals of 10 °C and its simultaneous influence on the product conversion and selectivity was studied. The results presented in Table S1† unambiguously revealed that among all the temperatures evaluated, 25 °C was found to be the most ideal one as it afforded the desired product with 100% conversion and selectivity.

Table 2 Synthesis of different β-enaminoesters and β-enaminones using Co-NQ@Am-SiO$_2$@Fe$_3$O$_4$ as the catalyst under solvent-free conditions[a]
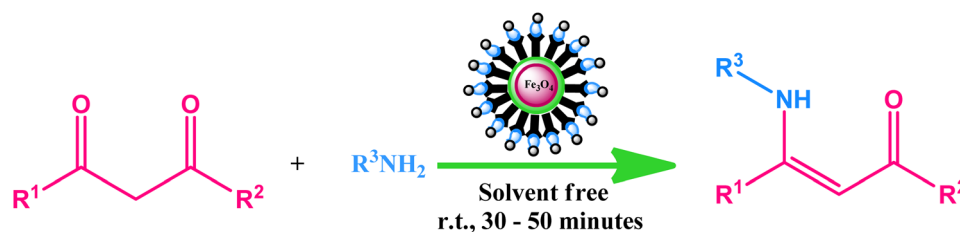
Entry	R^1	R^2	R^3	Conversion[b] (%)	Yield[c] (%)	TON[d]	TOF[e]
1	CH$_3$	OCH$_3$	CH$_2$Ph	100	95	357	714
2	CH$_3$	OCH$_3$	Ph	96	87	343	686
3	CH$_3$	OCH$_3$	4-CH$_3$Ph	95	90	339	678
4	CH$_3$	OCH$_3$	4-OCH$_3$Ph	86	82	307	614
5	CH$_3$	OCH$_3$	2-OCH$_3$Ph	80	80	286	572
6	CH$_3$	OCH$_3$	4-FPh	47	40	168	336
7	CH$_3$	OCH$_2$CH$_3$	CH$_2$Ph	98	91	350	700
8	CH$_3$	OCH$_2$CH$_3$	Ph	98	93	350	700
9	CH$_3$	OCH$_2$CH$_3$	4-CH$_3$Ph	95	86	339	678
10	CH$_3$	OCH$_2$CH$_3$	4-ClPh	61	55	218	436
11	CH$_3$	OCH$_2$CH$_3$	4-OCH$_3$Ph	88	81	314	628
12	CH$_3$	OCH$_2$CH$_3$	2-OCH$_3$Ph	67	59	239	478
13	Ph	OCH$_2$CH$_3$	PhCH$_2$	89	80	318	636
14	Ph	OCH$_2$CH$_3$	Ph	80	74	286	572
15	Ph	OCH$_2$CH$_3$	4-CH$_3$Ph	84	77	300	600
16	Ph	OCH$_2$CH$_3$	4-OCH$_3$Ph	78	69	279	558
17	Ph	OCH$_2$CH$_3$	2-OCH$_3$Ph	72	62	257	514
18	CH$_3$	OC(CH$_3$)$_3$	PhCH$_2$	91	79	325	650
19	CH$_3$	OCH$_2$Ph	PhCH$_2$	65	59	232	464
20	CH$_3$	OCH(CH$_3$)$_2$	PhCH$_2$	93	88	332	664
21	ClCH$_2$	OCH$_2$CH$_3$	PhCH$_2$	85	79	304	608
22	CF$_3$	OCH$_2$CH$_3$	PhCH$_2$	73	62	261	522
23	CH$_3$	CH$_3$	PhCH$_2$	100	95	357	714
24	CH$_3$	CH$_3$	4-ClPhCH$_2$	72	72	257	514
25	CH$_3$	CH$_3$	4-CH$_3$PhCH$_2$	87	85	311	622

[a] Reaction conditions: amine (1 mmol), β-ketoester (1 mmol), Co-NQ@Am-SiO$_2$@Fe$_3$O$_4$ catalyst (20 mg), stirring at r.t. (25 °C). [b] Conversion percentages determined via GC-MS have been given in parentheses. [c] Isolated yield. [d] TON is the number of moles of the product per mole of the catalyst. [e] TOF = TON/time (in Hours).

However, higher reaction temperatures (35 °C, 45 °C, 55 °C, and 65 °C) showed a noticeable decrease in the product selectivity which could be attributed to the formation of the di-substituted product.

Finally, the effect of reaction time on the percentage conversion of the model reactants was monitored by varying the time interval from 5 minutes to 30 minutes at 25 °C. The experimental results are displayed in Fig. S8.†

It is well apparent from the plot that the reaction conversion increases significantly with increasing the reaction time which is due to the fact that a longer time period favours the formation of the reactive intermediate species (substrate + catalyst) that eventually facilitates the formation of the desired product. A close inspection of the results showed that a reaction time of 30 minutes was the optimal period for the complete conversion of the model substrates.

Substrate scope and versatility

Pleased by the optimization results, we set out to challenge the capabilities of the Co-NQ@Am-SiO$_2$@Fe$_3$O$_4$ nanocatalyst in the synthesis of β-enaminones and β-enaminoesters (Table 2). In an endeavour towards envisaging the scope of this methodology, a wide array of β-ketoesters and β-diketones were reacted with several aromatic amines bearing electron rich as well as electron deficient substituents under the optimized reaction conditions. It was found that in general, the enamination reaction proceeded smoothly in the presence of the nano-structured cobalt catalyst *via* nucleophilic addition of amines to carbonyl compounds to afford the desired products with good to excellent conversion. However, the electronic factor played a key role in regulating the product conversion as evident from the results summarized in Table 2. The presence of electron withdrawing substituents such as F and Cl at the *para*-position of the benzene ring of the aromatic amines, in particular, resulted in a detrimental effect on the reaction conversion (Table 2, entries 6, 10, and 24). Also, in the case of aryl substituted β-ketoesters such as ethyl benzoylacetate, a moderate conversion was achieved despite continuing the reaction for a prolonged time period (Table 2, entries 13–17). Surprisingly, the rest of the β-ketoesters showed good reactivity and furnished the targeted product within a relatively shorter time. Notably, it is worth mentioning that although the

conversion percentage varied drastically depending on the nature of the substrate employed, all the reactions displayed excellent chemoselectivity.

In order to investigate the chemoselectivity of the process, we carried out a simple test (Scheme 2). First, we reacted a primary amine (*n*-butylamine) with β-ketoester (methylacetoacetate) under the optimized reaction conditions. We obtained the desired product with 70% reaction conversion. Next, we reacted a secondary amine (morpholine) with the same substrate (*i.e.* methylacetoacetate) and found that no morpholine derived product was formed even after prolonged stirring of the reaction contents.

Hot filtration test

For organic transformations involving a supported heterogeneous catalyst, an important issue that should be taken into account is the possibility of migration of the catalytically active species from the surface of the support material into the liquid phase during the course of the reaction. In order to exclude any catalytic contribution from the leached species, a standard hot filtration experiment was performed by subjecting the model reactants to vigorous stirring at room temperature in the presence of Co-NQ@Am-SiO$_2$@Fe$_3$O$_4$ (20 mg). At about half the reaction time (15 minutes), the catalyst was retrieved *via* magnetic decantation when the conversion percentage had reached 60% as estimated through GC-MS analysis. The resultant supernatant was allowed to react further for a prolonged time period under similar experimental conditions and the reaction progress was monitored continuously. No enhancement in the reaction conversion occurred even at extended times indicating that the active cobalt species remained tightly bound to the heterogeneous support. Additionally, atomic absorption and UV-visible spectroscopic analyses of the post reaction mixture were also carried out which showed the absence of cobalt in the supernatant as anticipated. The findings from all these studies synchronically provided concrete evidence for the heterogeneous nature of the catalyst.

Recyclability test

In green chemistry approaches for catalytic transformations, recovery and reusability are the two most significant attributes of a heterogeneous catalyst that lead to its large-scale industrial applicability. To assess the long-term stability and reusability of the synthesized nanostructured catalyst, we established a set of recycling experiments for the enamination reaction which were performed sequentially under the optimized reaction conditions using the test substrates. After completion of the first cycle, the solid catalyst was separated from the reaction vessel *via* magnetic attraction, washed with acetone several times to remove traces of the previous reaction mixture, dried under reduced pressure and thereafter subjected to a fresh run. Strikingly, it was found that the recovered nanocatalyst did not require the addition of any external reagent for getting reactivated. The results of the recycling test as demonstrated in Fig. 8 unveiled that Co-NQ@Am-SiO$_2$@Fe$_3$O$_4$ could be efficiently reused for eight consecutive trials without any
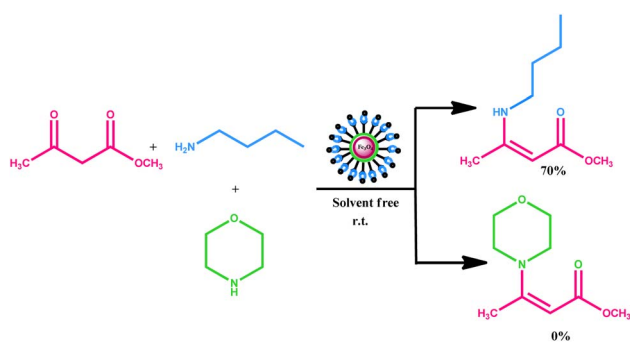
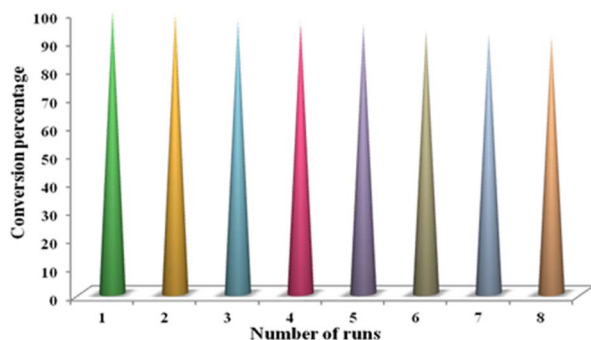**Scheme 2** Chemoselectivity test for the synthesis of β-enaminoesters.

Fig. 8 Recycling experiment for the enamination reaction [reaction conditions: benzylamine (1 mmol), methylacetoacetate (1 mmol), Co-NQ@Am-SiO$_2$@Fe$_3$O$_4$ catalyst (20 mg), stirring at r.t. (25 °C)].

substantial loss in its activity. Besides, the TEM micrograph of the recovered catalyst (obtained after the 8th run) provided key evidence for the structural durability of Co-NQ@Am-SiO$_2$@Fe$_3$O$_4$. It was found that its morphological characteristics remained largely preserved during the course of the reaction, signifying that the employed reaction conditions did not have any detrimental effect on its catalytic activity.

Comparison of the catalytic activity of Co-NQ@Am-SiO$_2$@Fe$_3$O$_4$ with that of the other reported heterogeneous catalysts

A comparison of the catalytic performance of Co-NQ@Am-SiO$_2$@Fe$_3$O$_4$ with the literature reported heterogeneous

Table 3 Comparison of the catalytic activity of Co-NQ@Am-SiO$_2$@Fe$_3$O$_4$ with that of previously reported heterogeneous catalysts for the enamination reaction

Entry	β-Ketoester/β-ketone	Amine	Catalytic system	Reaction conditions	Yield (%)	Ref.
1	H$_3$C–C(O)–CH$_2$–C(O)–OCH$_2$CH$_3$	aniline (NH$_2$)	[Cu(Hnbta)(1,3-btp)]·2H$_2$O Metal–organic-framework Recyclability: three runs	Solvent free r.t.	93	62
2	H$_3$C–C(O)–CH$_2$–C(O)–OCH$_2$CH$_3$	benzylamine (NH$_2$)	SiW/c-Al$_2$O$_3$ Supported heteropolyacid Recyclability: four runs	Acetonitrile r.t.	94	63
3	H$_3$C–C(O)–CH$_2$–C(O)–CH$_3$	aniline (NH$_2$)	Cu nanoparticles Recyclability: not evaluated	Methanol 45–50 °C under a N$_2$ atmosphere	92	64
4	H$_3$C–C(O)–CH$_2$–C(O)–CH$_3$	aniline (NH$_2$)	Silica sulfuric acid Recyclability: three runs	Solvent-free 80 °C	89	65
5	H$_3$C–C(O)–CH$_2$–C(O)–OCH$_2$CH$_3$	aniline (NH$_2$)	ZnO nanoparticles Recyclability: four runs	Solvent-free 80 °C	94	66
6	H$_3$C–C(O)–CH$_2$–C(O)–CH$_3$	aniline (NH$_2$)	NiO Recyclability: three runs	Ultrasound sonication 30 °C	90	67
7	H$_3$C–C(O)–CH$_2$–C(O)–OCH$_2$CH$_3$	aniline (NH$_2$)	Ag nanoparticles in hollow mesoporous spheres Recyclability: five runs	Methanol 60 °C	84	68
8	H$_3$C–C(O)–CH$_2$–C(O)–OCH$_2$CH$_3$	aniline (NH$_2$)	Silver nanoparticles Recyclability: three runs	Methanol 60 °C	70	69
9	H$_3$C–C(O)–CH$_2$–C(O)–OCH$_2$CH$_3$	aniline (NH$_2$)	Naphthoquinone cobalt complex supported on SiO$_2$@Fe$_3$O$_4$ nanoparticles Recyclability: eight runs	Solvent free r.t.	98	Present work
10	H$_3$C–C(O)–CH$_2$–C(O)–CH$_3$	aniline (NH$_2$)	Naphthoquinone cobalt complex supported on SiO$_2$@Fe$_3$O$_4$ nanoparticles	Solvent free r.t.	99	Present work

catalysts for the synthesis of biologically significant β-enaminones and β-enaminoesters is presented in Table 3. The results clearly demonstrate that the activity of Co-NQ@Am-SiO$_2$@Fe$_3$O$_4$ is far superior to that of the different heterogeneous catalytic systems reported so far[62–69] in terms of product yield, reaction conditions, durability and reusability. The reason behind the remarkable efficiency of the silica encapsulated magnetically retrievable cobalt catalyst can be attributed to the nanometer size of the support material which ensures greater binding of the substrates eventually leading to higher product yield. Furthermore, the ease of catalyst separation *via* simple magnetic attraction renders the protocol an attractive alternative for catalyzing the enamination of β-ketoesters and β-ketones as the magnetic field assisted separation prevents catalyst loss, reduces energy consumption and saves time in achieving catalyst recovery.

Conclusions

This work throws light on the synthesis of a new, versatile core–shell structured magnetically recoverable cobalt nanocatalyst that has been applied for the first time in the enamination of β-dicarbonyl compounds. The synthetic strategy adopted for preparing the catalyst is operationally simple and leads to the fabrication of a well configured nanostructure consisting of a naphthoquinone cobalt complex robustly anchored onto an amine functionalized silica encapsulated magnetite nanosupport. The as-synthesized nanocatalyst has been characterized well with the help of different spectroscopic and microscopic tools. XPS survey and core-level spectra of the obtained catalyst provide thorough evidence of the nature of the metal, showing that cobalt primarily existed in the +II oxidation state. This protocol impressively allows the generation of an appreciable range of the targeted molecules using the Co-NQ@Am-SiO$_2$@Fe$_3$O$_4$ nanocatalyst with excellent conversion (up to 100%) and a high turnover number (up to 357) at room temperature under solvent free conditions. In contrast to literature precedents for the enamination reaction, the present methodology offers a magnetically separable nanocatalyst that can be easily recovered from the reaction mixture with the help of an external magnet and reused further for several runs without any distinct loss in its activity. Besides, some of the other factors that worked towards enhancing the economic attractiveness of the protocol were its high atom economy, use of environmentally benign and inexpensive reagents, simple work up procedure, and mild reaction conditions. We strongly believe that the design of this high performance magnetically retrievable catalytic system would pave the pathway for future research aiming at development of new organic compounds of biological and industrial significance.

Author contributions

Sriparna Dutta was involved in designing, conceptualization, and experimental and writing work. Prashant Kumar was involved in writing and experimental work. Shivani Sharma and Priyanka helped in characterization and proofreading. Sneha

Yadav contributed to writing and data analysis. Ranjana Dixit, Anju Srivastava, and Rakesh Kumar Sharma were involved in overall monitoring and supervision.

Conflicts of interest

There are no conflicts to declare.

Acknowledgements

Notes and references

1 S. B. Kalidindi and B. R. Jagirdar, *ChemSusChem*, 2012, **5**, 65–75.

2 L. L. Chng, N. Erathodiyil and J. Y. Ying, *Acc. Chem. Res.*, 2013, **46**, 1825–1837.

3 V. Polshettiwar and R. S. Varma, *Green Chem.*, 2010, **12**, 743–754.

4 H. Barron and A. S. Barnard, *Catal. Sci. Technol.*, 2015, **5**, 2848–2855.

5 T. Mitsudome and K. Kaneda, *ChemCatChem*, 2013, **5**, 1681–1691.

6 D. Wang and D. Astruc, *Chem. Rev.*, 2014, **114**, 6949–6985.

7 L. M. Rossi, N. J. S. Costa, F. P. Silva and R. Wojcieszak, *Green Chem.*, 2014, **16**, 2906–2933.

8 V. Polshettiwar, R. Luque, A. Fihri, H. Zhu, M. Bouhrara and J.-M. Basset, *Chem. Rev.*, 2011, **111**, 3036–3075.

9 D. Zhang, C. Zhou, Z. Sun, L.-Z. Wu, C.-H. Tunga and T. Zhang, *Nanoscale*, 2012, **4**, 6244–6255.

10 R. B. N. Baig and R. S. Varma, *Chem. Commun.*, 2013, **49**, 752–770.

11 R. B. N. Baig and R. S. Varma, *Green Chem.*, 2013, **15**, 398–417.

12 S. Shylesh, V. Schünemann and W. R. Thiel, *Angew. Chem., Int. Ed.*, 2010, **49**, 3428–3459.

13 J. Govan and Y. K. Gunko, *Nanomaterials*, 2014, **4**, 222–241.

14 X. Gao, R. Liu, D. Zhang, M. Wu, T. Cheng and G. Liu, *Chem. Eur. J.*, 2014, **20**, 1515–1519.

15 S. Zheng, J. Sun, D. Song, Z. Chenab and J. Chen, *Chem. Commun.*, 2015, **51**, 11123–11125.

16 Y. Zhu, L. P. Stubbs, F. Ho, R. Liu, C. P. Ship, J. A. Maguire and N. S. Hosmane, *ChemCatChem*, 2010, **2**, 365–374.

17 Z. Wu, C. Sun, Y. Chai and M. Zhang, *RSC Adv.*, 2011, **1**, 1179–1182.

18 H. Yang, G. Li and Z. Ma, *J. Mater. Chem.*, 2012, **22**, 6639–6648.

19 S. Wang, Z. Zhang, B. Liu and J. Li, *Catal. Sci. Technol.*, 2013, **3**, 2104–2112.

20 C. Jin, Y. Wang, H. Wei, H. Tang, X. Liu, T. Lua and J. Wang, *J. Mater. Chem. A*, 2014, **2**, 11202–11208.

21 I. O. Edafiogho, S. B. Kombian, K. V. Ananthalakshmi, N. N. Salama, N. D. Eddington, T. L. Wilson, M. S. Alexander, P. L. Jackson, C. D. Hanson and K. R. Scott, *J. Pharm. Sci.*, 2007, **96**, 2509–2531.

22 M. Abass and B. B. Mostafa, *Bioorg. Med. Chem.*, 2005, **13**, 6133–6144.

23 A. M. Ei-Shennawy, A. H. Mohamed and M. Abass, *MedGenMed*, 2007, **9**, 15–33.

24 J. D. White and D. C. Ihle, *Org. Lett.*, 2006, **8**, 1081–1084.

25 N. N. Salama, K. R. Scott and N. D. Eddington, *Biopharm. Drug Dispos.*, 2004, **25**, 227–236.

26 N. D. Eddington, D. S. Cox, M. Khurana, N. N. Salama, J. P. Stables, S. J. Harrison, A. Negussie, R. S. Taylor, U. Q. Tran, J. A. Moore, J. C. Barrow and K. R. Scott, *Eur. J. Med. Chem.*, 2003, **38**, 49–64.

27 A. P. Marcus and R. Sarpong, *Org. Lett.*, 2010, **12**, 4560–4563.

28 J. P. Michael, C. B. Koning, G. D. Hosken and T. V. Stanbury, *Tetrahedron*, 2001, **57**, 9635–9648.

29 I. O. Edafiogho, M. S. Alexander, J. A. Moore, V. A. Farrar and K. R. Scott, *Curr. Med. Chem.*, 1994, **1**, 159–175.

30 Y. F. Wang, T. Izawa, S. Kobayashi and M. Ohno, *J. Am. Chem. Soc.*, 1982, **104**, 6465–6466.

31 D. L. Boger, T. Ishizaki, J. R. Jr Wysocki, S. A. Munk, P. A. Kitos and O. Suntornwat, *J. Am. Chem. Soc.*, 1989, **111**, 6461–6463.

32 G. Cimarelli, G. Palmieri and E. Volpini, *Tetrahedron Lett.*, 2004, **45**, 6629–6631.

33 K. Uneyama, O. Morimoto and F. Yamashita, *Tetrahedron Lett.*, 1989, **30**, 4821–4824.

34 S. Fustero, B. Pina, A. Simo and N. Fuentes, *Tetrahedron Lett.*, 1997, **38**, 6771–6774.

35 S. Fustero, B. Pina, E. Salavert, A. Navarro, C. RamTrez de Arellano and A. Simón, *J. Org. Chem.*, 2002, **67**, 4667–4679.

36 S. Fustero, B. Pina, M. GarcTa de la Torre, A. Navarro, C. Ramirez de Arellano and A. Simón, *Org. Lett.*, 1999, **1**, 977–980.

37 S. M. Hannick and Y. Kishi, *J. Org. Chem.*, 1983, **48**, 3833–3835.

38 A. S.-Y. Lee and R.-Y. Cheng, *Tetrahedron Lett.*, 1997, **38**, 443–446.

39 T. G. C. Bird and A. Olivier, *Bioorg. Med. Chem. Lett.*, 1996, **6**, 515–520.

40 T. Fukuyama and Y. M. Yung, *Tetrahedron Lett.*, 1981, **22**, 3759–3760.

41 N. Jiang, Z. Qu and J. Wang, *Org. Lett.*, 2001, **3**, 2989–2992.

42 G. Bartoli, C. Cimarelli, R. Dalpozzo and G. Palmieri, *Tetrahedron*, 1995, **51**, 8613–8622.

43 A. R. Katritzky, Y. Fang, A. Donkor and J. Xu, *Synthesis*, 2000, 2029–2032.

44 S. Fustero, M. GarcTa de la Torre, V. Jofre`, R. Pérez Carlon, A. Navarro and A. Simón Fuentes, *J. Org. Chem.*, 1998, **63**, 8825–8836.

45 D. F. Martin, G. A. Janusonis and B. B. Martin, *J. Am. Chem. Soc.*, 1961, **83**, 73–75.

46 J. S. Yadav, V. N. Kumar, R. S. Rao, A. D. Priyadarshini, P. P. Rao, B. V. S. Reddy and K. Nagaiah, *J. Mol. Catal. A: Chem.*, 2006, **256**, 234–237.

47 R. K. Vohra, J. L. Renaud and C. Bruneau, *Collect. Czech. Chem. Commun.*, 2005, **70**, 1943–1952.

48 Z. H. Zhang, T. S. Li and J. J. Li, *Catal. Commun.*, 2007, **8**, 1615–1620.

49 M. A. Harrad, R. Outtouch, M. A. Ali, L. El Firdoussi, A. Karim and A. Roucoux, *Catal. Commun.*, 2010, **11**, 442–446.

50 Z. H. Zhang and J. Y. Hu, *J. Braz. Chem. Soc.*, 2006, **17**, 1447–1451.

51 Z. H. Zhang, L. Yin and Y. M. Wang, *Adv. Synth. Catal.*, 2006, **348**, 184–190.

52 S. Gogoi, R. Bhuyan and N. C. Barua, *Anal. Lett.*, 2005, **35**, 2811–2818.

53 Y. Gao, Q. Zhang and J. Xu, *Synth. Commun.*, 2004, **34**, 909–916.

54 M. M. Khodaei, A. R. Khosropour and M. Kookhazadeh, *Synlett*, 2004, **11**, 1980–1984.

55 A. Arcadi, G. Bianchi, S. Di Giuseppe and F. Marinelli, *Green Chem.*, 2003, **5**, 64–67.

56 V. Polshettiwar, B. Baruwati and R. S. Varma, *Green Chem.*, 2009, **11**, 127–131.

57 Q. Zhang, H. Su, J. Luo and Y. Wei, *Green Chem.*, 2012, **14**, 201–208.

58 Z. Afrasiabi, E. Sinn, P. P. Kulkarni, V. Ambike, S. Padhye, D. Deobagakar, H. Mark, G. Chris, E. A. Christopher and A. K. Powell, *Inorg. Chim. Acta*, 2005, **358**, 2023–2030.

59 K. Petcharoena and A. Sirivat, *Mater. Sci. Eng., B*, 2012, **177**, 421–427.

60 S. Wang, Z. Zhang, B. Liu and J. Li, *Catal. Sci. Technol.*, 2013, **3**, 2104–2112.

61 M. Esmaeilpour, A. R. Sardarian and J. Javidi, *J. Organomet. Chem.*, 2014, **749**, 233–240.

62 Y. Zhao, D. S. Deng, L. F. Ma, B. M. Ji and L. Y. Wang, *Chem. Commun.*, 2013, **49**, 10299–10301.

63 E. Rafiee, M. Joshaghani, S. Eavani and S. Rashidzadeh, *Green Chem.*, 2008, **10**, 982–989.

64 M. Kidwai, S. Bhardwaj, N. K. Mishra, V. Bansal, A. Kumar and S. Mozumdar, *Catal. Commun.*, 2009, **10**, 1514–1517.

65 A. Hasaninejad, A. Zare, M. R. Mohammadizadeh, M. Shekouhy and A. R. Moosavi-Zare, *J. Chem.*, 2010, **7**, 1546–1554.

66 U. U. Indulkar, S. R. Kale, M. B. Gawande and R. V. Jayaram, *Tetrahedron Lett.*, 2012, **53**, 3857–3860.

67 S. Shendage and J. Nagarkar, *Curr. Chem. Lett.*, 2013, **2**, 145–152.

68 J. Sun, Z. Dong, P. Li, F. Zhang, S. Wei, Z. Shi and R. Li, *Mater. Chem. Phys.*, 2013, **140**, 1–6.

69 K. D. Bhatte, P. J. Tambade, K. P. Dhake and B. M. Bhanage, *Catal. Commun.*, 2010, **11**, 1233–1237.